


## Article

# Structural Insights into Phycocyanin Langmuir–Blodgett Multilayers via Serial Femtosecond Crystallography with X-ray Free-Electron Laser

Eugenia Pechkova <sup>1,\*</sup>, Fabio Massimo Speranza <sup>2</sup>, Paola Ghisellini <sup>3</sup>, Stefano Fiordoro <sup>4</sup> , Cristina Rando <sup>3</sup> and Roberto Eggenhöfner <sup>3,\*</sup> 

<sup>1</sup> Laboratories of Biophysics and Nanotechnology, Department of Experimental Medicine (DIMES), University of Genova Medical School, Via A. Pastore, 3, 16132 Genova, Italy

<sup>2</sup> Independent Researcher, 16147 Genova, Italy; fabiom.speranza@gmail.com

<sup>3</sup> Department of Surgical Sciences and Integrated Diagnostics (DISC), Genova University, Corso Europa 30, 16132 Genova, Italy; paola.ghisellini@unige.it (P.G.); cristina.rando@unige.it (C.R.)

<sup>4</sup> Department of Health Science (DISSAL), University of Genova Medical School, 16132 Genova, Italy; stefano.fiordoro@edu.unige.it

\* Correspondence: epechkova@nwi.unige.it (E.P.); roberto.eggenhoffner@unige.it (R.E.)

**Abstract:** Serial femtosecond crystallography (SFX) with X-ray free-electron lasers (XFELs) has revolutionized classical X-ray diffraction experiments by utilizing ultra-short, intense, and coherent X-ray pulses. However, the SFX approach still requires thousands of nearly identical samples, leading to significant protein consumption. We propose utilizing Langmuir–Blodgett protein multilayers, which are characterized by long-range order, thermal stability, and the ability to induce protein crystallization, even in proteins that cannot be crystallized by conventional methods. This study aimed to combine the intrinsic properties of Langmuir–Blodgett multilayers with advanced XFEL techniques at the Linac Coherent Light Source. Since the macromolecule organization can be explored in nano or 2D crystals exploiting the properties of SFX–XFEL radiation that enable the capture of high-resolution diffraction images before radiation damage occurs, we propose Langmuir–Blodgett protein nanofilm technology as a novel approach for direct “on-chip” protein sample preparation. The present study extends previous investigations into Langmuir–Blodgett phycocyanin multilayer nanofilms using synchrotron radiation cryo-EM microscopy and second-order nonlinear imaging of chiral crystal (SONICC) experiments. We also examined the thermal stability of phycocyanin Langmuir–Blodgett multilayered films deposited on Si<sub>3</sub>N<sub>4</sub> membranes to evaluate structural changes occurring at 150 °C compared with room temperature. Phycocyanin Langmuir–Blodgett films are worthy of investigation in view of their suitability for tissue engineering and other applications due to their thermal integrity and stability as the results of the present investigation reveal.

**Keywords:** phycocyanin crystals; Langmuir–Blodgett films; serial femtosecond crystallography; X-ray-free electron laser; protein thermal stability



**Citation:** Pechkova, E.; Speranza, F.M.; Ghisellini, P.; Fiordoro, S.; Rando, C.; Eggenhöfner, R. Structural Insights into Phycocyanin Langmuir–Blodgett Multilayers via Serial Femtosecond Crystallography with X-ray Free-Electron Laser. *Crystals* **2024**, *14*, 767. <https://doi.org/10.3390/cryst14090767>

Academic Editor: Ki Hyun Nam

Received: 6 August 2024

Revised: 23 August 2024

Accepted: 26 August 2024

Published: 29 August 2024



**Copyright:** © 2024 by the authors. Licensee MDPI, Basel, Switzerland. This article is an open access article distributed under the terms and conditions of the Creative Commons Attribution (CC BY) license (<https://creativecommons.org/licenses/by/4.0/>).

## 1. Introduction

Phycocyanin, a Phycobiliprotein present in cyanobacteria and red algae, is a pigment–protein complex that is vital to photosynthesis [1]. Phycobiliproteins are part of phycobilisome–supramolecular complexes, which constitute the light-harvesting antennae for oxygenic photosynthesis in cyanobacteria (blue-green algae) and red algae [2–4]. Phycocyanin’s strong light absorption makes it highly useful for biophotonics and biosensing applications, as a natural dye in food and cosmetics, and even as a potential cancer treatment drug [5]. However, such applications often require specific operating conditions, with thermal stability being one of the most critical. Several advanced methods, such as cryo-EM, X-ray nanodiffraction, and XFEL were previously used for probing local temperature-induced self-assembly in thermally annealed PC LB multilayered nanofilms [6].

The Langmuir–Blodgett (LB) technique is a method used to fabricate thin films with highly controlled thickness and composition by depositing molecular layers onto a solid substrate via transfer from the air–water interface [7]. The LB method produces uniform, well-organized nanoscale structures, leading to a wide range of applications for these films [8]. In biophysics and tissue engineering, where materials are often exposed to varying temperatures, the thermal stability of LB films is crucial.

Proteins, being sensitive to heat, can undergo denaturation or aggregation when exposed to high temperatures, leading to losses of functionality and structural integrity. Previous studies on the thermal stability of protein LB films have shown that certain proteins can maintain their structure at relatively high temperatures when organized within these films. Moreover, an increase in the long-range order in the LB multilayered protein films after heating and cooling, made previously apparent by  $\mu$ GISAX synchrotron radiation experiments [9], was studied by powder X-ray diffraction studies and resulted in clear appearance in the 2D and 3D space, respectively, of the diffraction peaks typical of the corresponding protein crystal structure [10]. These results were confirmed by recent investigations using nano-X-ray diffraction (nano-XRD) in transmission mode, revealing the emergence of amyloid fibrillation in 2D-ordered LB protein multilayers upon heating [11]. The thermal stability and aggregation of C-phycoerythrin were also recently studied by light scattering and fluorescence [12]. Nevertheless, the unique thermal behavior of phycoerythrin LB multilayers, particularly when subjected to high temperatures, is an issue that remains poorly understood. In order to fill this knowledge gap, this work aimed at investigating the thermal stability of multilayered films of phycoerythrin LB deposited on a  $\text{Si}_3\text{N}_4$  membrane and performing detailed structural analysis before and after thermal treatment. Our objective was to evaluate the structural changes in these films, heated to 150 °C and then cooled back down to room temperature. Thermal annealing of phycoerythrin LB multilayers already yielded encouraging results when studied using cryo-electron microscopy in its micro-electron diffraction (micro-ED) mode [6]. Here, we employed for our investigation serial femtosecond crystallography (SFX) with the X-ray-free electron laser (XFEL) at the Linac Coherent Light Source (LCLS) at SLAC National Accelerator Laboratory. In contrast to conventional X-ray sources, which can cause significant radiation damage during data collection, SFX methods with XFELs are characterized by ultra-short femtosecond pulses that allow for the collection of diffraction data before damage occurs. This SFX technique is well known for capturing high-resolution diffraction patterns from a large number of microcrystals, each exposed to a single pulse, thus avoiding cumulative damage and enabling the study of highly radiation-sensitive and small crystals. Serial femtosecond crystallography with XFELs has thus become an important tool for the structural determination of proteins that are difficult to crystallize, such as membrane proteins, as well as for time-resolved structural studies [13–15].

Several sample delivery methods have been developed for SFX experiments with XFELs [16]. Firstly, a suspension of micro- or nanocrystals is delivered to the X-ray beam using a continuous liquid jet with aerodynamic focusing of its diameter down to a few micrometers [17]. Common drawbacks include nozzle clogging by larger crystals, which must be filtered before the experiment, and high sample consumption, with hit rates typically around 10%, although better results have been achieved with “toothpaste”-like lipidic cubic phase (LCP) jets [18,19]. However, delicate crystals may be damaged from the pressures and shear forces of the delivery process itself, and neither method is suitable for few-layer crystals.

Another method for fast sample delivery with XFELs involves the use of fixed substrates, which are mounted on mechanical translation stages and raster-scanned through the beam. The micro-patterned structure of the chip facilitates automatic measurements by raster scanning of the individual wells of the chip, where the crystals arrange themselves in a periodic array. The technology uses photolithography masks and includes a number of approaches also suitable for 2D crystal analysis [20–22]. The drawback of fixed-target approaches is usually an increase in background scattering that arises from the relatively

thick (>50 nm) device material layer that can interfere with weak diffraction patterns. Another problem is that the crystals must be removed from their native-growth condition.

XFEL data collection in transmission geometry through ultrathin Si<sub>3</sub>N<sub>4</sub> membranes (also commercially available) allows an extremely low scattering background, which is ideal for nanocrystals scattering experiments. The XFEL scans provide high-resolution diffraction images of the samples deposited on these membranes, allowing detailed structural analysis [23]. In the present work, we propose the potential advances in fixed target developments that could allow direct “on-chip” protein molecule diffracting assembly, which would simplify the overall procedure, avoiding harvesting and sample overconsumption. Highly ordered protein LB multilayers were used in a diffraction experiment in order to obtain a diffraction pattern directly from the deposited film, thermally annealed to 150 °C.

Data obtained from X-ray free-electron lasers (XFELs) present significant challenges for traditional data reduction software [24]. Several analytic software programs are available for analyzing crystallographic data at free-electron laser facilities, including Cheetah [25], OnDA [26,27], IOTA [28], CASS [29], and Psocake [30]. In the present work, the latter was used for the analyses of XFEL data collected from LB multilayers.

## 2. Materials and Methods

### 2.1. Protein Sample Preparation

The native phycocyanin protein was obtained by Dr. Raimund Fromme, from cyanobacteria *Thermosynechococcus elongates*, as described by Fromme et al., 2015 [31]. Cells were pre-processed with a microfluidizer to break the cell walls, followed by centrifugation to isolate the thylakoid membrane. Phycobiliproteins such as phycocyanin were isolated by ultracentrifugation; the supernatant was concentrated using Centricon spin filters with a molecular-weight cutoff of 100 kDa to obtain protein at 50 mg/mL. Purity and integrity were confirmed by SDS-PAGE and UV-Vis spectroscopy analysis, with absorption peaks at 620 nm indicating high purity [32]. Thermal stability tests showed the protein withstands temperatures up to 50 °C without significant loss of properties [33,34].

### 2.2. Protein LB Film Deposition

Phycocyanin LB films were prepared using the LB technique, with experimental details reported in reference [35]. The Si chip, measuring 10 × 10 mm<sup>2</sup> with silicon nitride Si<sub>3</sub>N<sub>4</sub> membrane windows of 5 × 5 mm<sup>2</sup> and a thickness of 200 nm (Silson Ltd., Warwickshire, UK), was used as a substrate for depositing phycocyanin multilayers. These membranes were chosen for their low background signal, making them suitable for X-ray experiments in transmission geometry. LB nanofilms were deposited using a Nima 611 LB trough equipped with a Teflon bath. Proper conditions for ordered LB film deposition were determined, taking into account factors such as the composition of the subphase, the speed of the barriers, and the surface pressure during deposition [8]. The protein solution at a 10 mg/mL concentration was spread onto the subphase surface of the Langmuir trough using a Hamilton syringe. The monolayer was compressed at a surface pressure of 26 mN/m using movable barriers.

The Silson slide was securely held by a vacuum apparatus (Hampton research, Aliso Viejo, CA, USA, HR8-098). The monolayers formed in the previous step were transferred onto the Si<sub>3</sub>N<sub>4</sub> membrane by horizontally dipping and withdrawing the substrate through the monolayer (Langmuir–Schaeffer method), repeating this process to build up the desired number of layers. Each monolayer that was deposited was dried using nitrogen flux before the next deposition.

We prepared LB multilayers nanofilms, with each one consisting of 20 monolayers, by repeatedly transferring the monolayer from the air–water interface to the Si<sub>3</sub>N<sub>4</sub> substrate.

The prepared samples were divided into two groups—one group of samples were held at room temperature, while the second group underwent thermal annealing. These samples

were heated to 150 °C using a controlled heating apparatus for 10 min to ensure uniform heating. After heating, the samples were allowed to cool back to room temperature.

### 2.3. XFEL Experiments and Data Collection

XFEL experiments were conducted at the LCLS, SLAC, USA. We used a Roadrunner II goniometer developed in-house at the SLAC National Accelerator Laboratory with a macromolecular femtosecond X-ray crystallography (MFX) instrument and a CSPAD detector frame rate of 120 Hz. The CSPAD detector (Cornell–SLAC Pixel Array Detector, Cornell, CA, USA) is the first detector specifically developed for use at LCLS as the result of the collaboration between Cornell University and the SLAC National Accelerator Laboratory. The detector frame rate was 120 Hz, while the detector distance was 313 mm. We used 6–9 keV, ~20 fs X-ray pulses, and  $1 \times 2 \mu\text{m}^2$  beam size for LB multilayers. Data collection modes for SFX included raster scanning (automated translation of the sample between exposures). Unlike the usual diffraction-before-destruction experiment, where the sample is introduced into the trajectory of the X-ray beam using either a continuous liquid stream or a suspension of fine particles, we applied the fixed-target approach, which consists of consecutive displacements of the sample with the translation of 90  $\mu\text{m}$ , in such a way that the X-ray beam always hits a new portion of the sample at a distance of 90  $\mu\text{m}$  from each other. All data collection was performed at room temperature.

In order to securely attach the Silson slides to the Roadrunner II goniometer, they were affixed to an aluminum frame. This frame was placed on the goniometer using a magnetic mount. Once the chip was attached to the goniometer, it was positioned with its edge facing the camera. Then, it was positioned in the X-ray interaction zone, which was also the center of rotation for the microdiffractometer. Since dehydration was not a concern for the dry LB films, there was no need to use a stream of humidified helium or any comparable process. Nevertheless, humidity sensors were employed to quantify the humidity levels during the experiment.

Initial XFEL scans were performed on the  $\text{Si}_3\text{N}_4$  membrane itself and LB films stored at room temperature to establish a baseline. This provided as a point of reference for evaluating any modifications brought about by heat treatment. Then, thermally annealed samples were analyzed.

### 2.4. XFEL Data Analysis

SFX–XFEL-collected data were analyzed using Psocake, a software package that includes a graphical user interface (GUI). It was applied for adjusting peak parameters and running SFX analysis operations on computing clusters at the free-electron laser facility at SLAC. Psocake has been created as a new approach, integrating novel concepts and ideas from preexisting technologies [30]. The Psocake software and its algorithms can be accessed for free from our Github repository at [www.github.com/lcls-psana/psocake](https://www.github.com/lcls-psana/psocake) (accessed on 24 August 2024).

## 3. Results and Discussion

A total of 22,920 images were collected from the room-temperature-stored samples, and 22,080 images were collected from the thermally annealed samples of the LB phycocyanin multilayers. The scans were analyzed to identify any structural changes or defects in the LB films after the temperature treatment.

With Psocake software version v.1.0.15, we detected the quantity of peaks in each frame using the possibility of adjusting the peak-finding settings with quick updates to the peak finding on the Image Viewer panel. For example, if any Bragg spots were not detected, we analyzed the intensity data over the specific pixel to reveal their position and intensity. The frame was therefore classified as a hit if it had more than 15 peaks. This categorization significantly reduced the computational requirements in the subsequent stages of the processing pipeline. A specific customized mask was applied on defective pixels in order to exclude them from the analysis. After masking and peak finding, the geometry optimization

took place in the data analysis. Four different files (max.npy, mean.npy, std.npy, sum.npy) were generated, and max or std files were mostly used. Generating these files improved the overall geometry for data processing. Control experiments were conducted using empty chips and SiN<sub>4</sub> windows without samples to establish a baseline for background noise and artifacts, as reported above. These control runs were critical for understanding the contributions of the substrate and experimental setup. No significant diffraction patterns were observed in these two control runs, confirming that any detected spots in the other experimental runs were attributed to the phycocyanin samples rather than the substrate or equipment.

The initial scans of the phycocyanin LB multilayered film on the Si<sub>3</sub>N<sub>4</sub> membrane showed a uniform grid pattern, indicating a consistent and defect-free substrate. This uniformity was crucial for ensuring the reliable and reproducible deposition of the LB films. The phycocyanin LB films exhibited a well-defined multilayer structure, essential for the subsequent thermal stability analysis (Figure 1a).

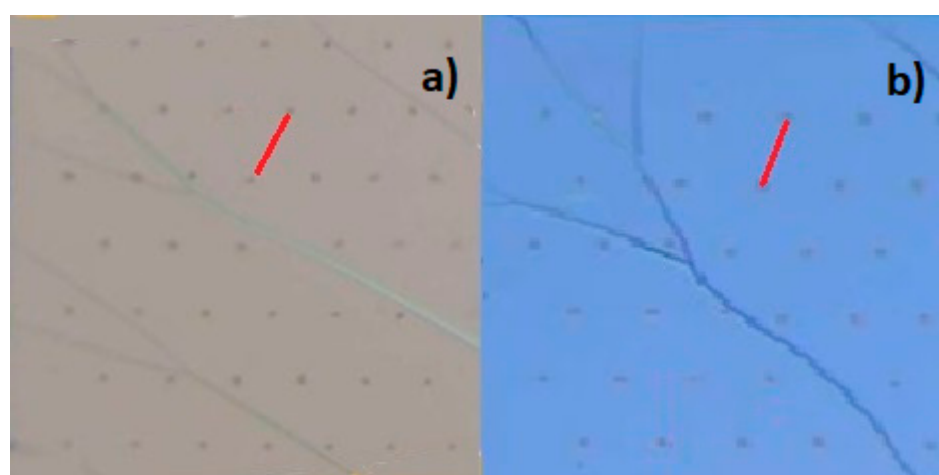


**Figure 1.** XFEL scanning of Si<sub>3</sub>N<sub>4</sub> membrane and phycocyanin LB multilayered film. (a) XFEL scan of the Si<sub>3</sub>N<sub>4</sub> membrane that was 200 nm thick with phycocyanin LB film at room temperature. The scan shows a uniform grid pattern, indicating a consistent and defect-free substrate with well-organized multilayers. (b) XFEL scan of the phycocyanin LB multilayered film (20 monolayers), heated up to 150 °C and cooled down to room temperature. The red line is 90 μm long in both panels.

The scans taken after heating to 150 °C and cooling back to room temperature revealed that the phycocyanin LB films maintained their structural integrity. While some cracks and lines were observed, these were minimal and did not significantly disrupt the overall multilayer structure.

The images in Figure 2 show the X-ray diffraction patterns obtained from the phycocyanin LB (20 multilayers) films, with one set of patterns (Figure 2a) recorded at room temperature (RT) and the other (Figure 2b) at RT but after being heated to 150 °C and cooled down to room temperature. Both images display sharp and well-defined diffraction spots, indicating the presence of the well-ordered domains of crystalline structures, due to the Bragg diffraction of XFEL rays from the regularly spaced planes on the film surface. Similar spots, though more numerous for 30%, are seen in the pattern of Figure 2b after heating to 150 °C in comparison to the film kept at room temperature. This suggested that the crystalline order was preserved after the heating treatment. The stability of the phycocyanin LB films during thermal annealing (TA) was indicated by the preservation of diffraction spots after the high-temperature treatment. The latter process produced a higher number of distinct diffraction spots by presumably reducing defects, merging smaller crystalline domains into larger ones, and improving the packing order of protein molecules. The labeled rings in the diffraction patterns in Figure 2 correspond to different resolutions, measured and reported in angstroms (Å), corresponding to different levels of structural



detail resolved in the crystal. In SFX, the outer rings indicate higher resolution (lower Å values), which correspond to finer structural details, while the inner rings represent lower resolution (higher Å values), indicating broader structural features. The ultra-short and coherent pulses from the XFEL enabled the detection of high-resolution data, limited by the detector's spatial resolution and the intrinsic order of the sample.

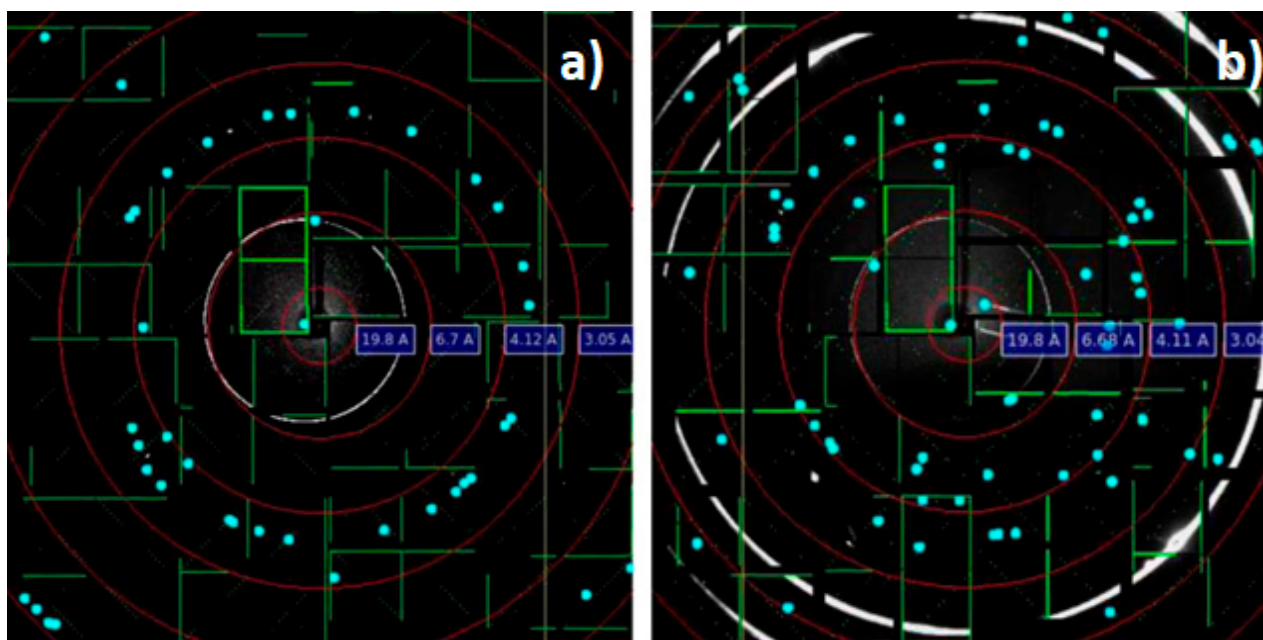


**Figure 2.** XFEL scanning of phycocyanin LB multilayered films. (a) XFEL scan of the phycocyanin LB multilayered film (20 monolayers) at room temperature. The scan shows a uniform grid pattern, indicating a consistent and defect-free substrate with well-organized multilayers. (b) XFEL scan of the phycocyanin LB multilayered film (20 monolayers) after being heated to 150 °C and cooled down to room temperature. The scan reveals numerous diffraction spots, indicating enhanced crystallization within the multilayered film after thermal treatment. The cyan color indicates the diffraction spots that are identified by clusters of predetermined number of detector's pixels.

When considering SFX using an X-ray free-electron laser (XFEL), there are additional aspects of the physics and methodology that enhance our understanding of resolution rings and diffraction patterns. XFELs produce extremely short pulses (in the order of femtoseconds, seconds), allowing the capture of diffraction images before significant radiation damage occurs to the sample. The intense X-ray beams generated by XFELs enable the diffraction of even very small crystals, which might not diffract strongly with conventional X-ray sources. In SFX, thousands to millions of diffraction patterns are collected from many microcrystals, each exposed to a single femtosecond pulse, avoiding the accumulation of radiation damage. High-coherence X-ray beams are produced by XFELs, which improve the diffraction patterns' contrast and quality. The resolution in X-ray crystallography is determined by the interplanar spacing  $d$ , where lower  $d$  values correspond to higher resolution. According to Bragg's law ( $n\lambda = 2d\sin\theta$ ), higher scattering angles  $2\theta$  correlate with lower  $d$  values, thus higher resolution. In our SFX experiments, the high coherence and intensity of the XFEL beams allowed us to resolve finer details in the crystal structure. The concentric rings in the diffraction patterns indicate reflections from sets of parallel planes with different  $d$  spacings. Outer rings, which correspond to higher scattering angles, represent higher resolution and are more easily observed due to the high signal-to-noise ratio provided by XFELs. This high-resolution capacity is essential for thorough structural analysis, especially with difficult biological materials. Due to the high intensity and coherence of XFELs, higher-resolution data can be obtained, often limited by the detector's spatial resolution and the sample's intrinsic order.

The thermal stability of the phycocyanin LB films was evidenced by the minimal structural changes observed in the XFEL scans after thermal treatment. The Si<sub>3</sub>N<sub>4</sub> membrane provided a stable substrate, ensuring that any observed changes were attributable to the LB films themselves. The preservation of the grid pattern and the minimal appearance of cracks indicated that the films could withstand significant thermal stress without substantial degradation.

The spots in relation to the ring were quantified, as reported in Table 1; the number of diffraction spots within these circle rings is indicative of the crystalline quality of the phycocyanin LB films.

**Table 1.** At room temperature (RT) and after the thermal annealing (TA) cycle.

Ring Resolution (Å)	RT Spots	TA Spots	% Difference
19.8	2	5	+60%
6.7	3	22	+87%
4.12	28	24	−17%
>3.05	8	16	+50%

In the innermost circle (19.8 Å), we had the lowest number of spots, although prevailing from the TA treatment for 60%. The slight increase in the number of spots at 150 °C indicated a modest improvement in the crystallinity for low-resolution features. This suggests that TA has a positive effect even on broader structural features, making them more discernible, still at a relatively low degree of long-range crystallization. In the second circle from the center (6.7 Å), we had similar findings to the RT number of spots with respect to the innermost circle, and, on the contrary, a much higher number of spots from the TA films in this circle. Such a substantial increase in the number of spots in TA highlights a significant enhancement in the medium-resolution structural details after TA, resulting in a process capable of effectively reorganizing the protein molecules into a more ordered state, greatly improving the medium-range order in the crystal structure. In the third circle (4.12 Å), we detected the highest number of spots, both at RT and after TA, indicating that the LB film preparation led to the highest degree of crystallization within the resolution range of approximately between 3 and 4 Å. Furthermore, the RT spots prevailed only in this range, though only slightly. This finding indicates that while the TA process improves medium- to high-resolution features, it might also cause some redistribution of the crystalline domains, leading to a slight reduction in spot count at this resolution. Finally, for the outer circle (>3.05 Å), we detected fewer spots at RT and after TA, with a more marked reduction in the RT films. The doubling of spots in the highest-resolution ring (>3.05 Å) after annealing indicates a significant improvement in the high-resolution structural details. This implies that the thermal treatment enhanced the fine atomic-level order within the crystal, making it more suitable for detailed structural analysis. The RT films showed a lower degree of such high-resolution structural details. Overall, the increase in the number of spots with TA treatment for most resolution ranges (particularly at 6.7 Å and >3.05 Å) clearly indicated that the TA process enhanced the overall crystallinity of the phycocyanin LB multilayer films and promoted the formation of larger, more coherent crystalline domains, improvements crucial for obtaining high-quality diffraction data. This underscores the benefits of thermal treatment in preparing high-quality crystalline samples for advanced structural analysis using techniques such as XFEL. The fact that the number of high-resolution spots increases (or remains high) after TA suggests that LB films are thermally stable and that TA can be an effective method for improving their structural properties. These findings support the use of annealed LB films for high-resolution structural studies, as enhanced crystallinity will enable better data quality for protein structure determination and improved biophysical research applications. Furthermore, these results align with the results obtained in protein LB films studied through grazing-incidence small-angle X-ray scattering technique using a microfocus beamline (μGISAXS) [9].

The ability of the LB films to maintain and even improve their diffraction quality during the TA treatment confirmed their thermal stability. The demonstrated thermal stability and improved crystallization of Phycocyanin LB films extend the variety of biophysical experiments and industrial processes in which they can be used. In biophotonics, for instance, where precise and stable light absorption and emission properties are required, the ability to maintain and improve structural integrity under thermal stress is critical [36]. Similarly, in tissue engineering, where materials may be subjected to body temperature fluctuations or external thermal treatments, such stability and improved crystallization ensure reliable and enhanced performance [37]. The results reported in Figure 2 and Table 1 point out that LB preparation intrinsically favors the reorganization of phycocyanin molecules into a more ordered state, in particular after a heating and cooling procedure, proving the robustness of phycocyanin LB films. We suggest that this stability is basically caused by the strong intermolecular interactions among the phycocyanin molecules since heating facilitates the reduction in internal stresses within the nanofilms, leading to an augmentation in the molecular packing density and a subsequent improvement in the crystallinity. This thermal treatment allows the molecules to overcome local minima in their energy landscape, thereby enabling them to attain a more thermodynamically stable configuration. This effect was confirmed by both quartz crystal microbalance (QCM) measurements, which indicated a consistent increase in mass due to higher molecular density packing, and by atomic force microscopy (AFM) imaging, which revealed a more uniform and tightly packed crystal structure after heating [9].

#### 4. Conclusions

Using the X-ray free-electron laser (XFEL) at the LCLS, we performed SFX to obtain high-resolution diffraction data from phycocyanin LB multilayer films. Phycocyanin LB multilayered films demonstrated high thermal stability and enhanced crystallization when subjected to temperatures up to 150 °C, making them suitable for high-resolution structural studies and various biophysical applications.

Future studies could examine how well these films perform in different environments and concentrate on detailed mechanistic understandings of their thermal resilience and crystallization behavior. The specific mechanisms underlying the enhanced crystallization of phycocyanin LB films subjected to thermal treatment could be investigated in more detail. Investigating the role of intermolecular interactions, film thickness, and substrate properties may provide additional insight into the factors influencing the observed stability and crystallization and, additionally, examining the behavior in different environmental conditions.

**Author Contributions:** Conceptualization: E.P., R.E.; methodology, P.G., S.F., C.R.; software and data curation: F.M.S.; data reduction and analysis: E.P., F.M.S.; validation and formal analysis, E.P., R.E.; writing—original draft preparation, E.P., F.M.S., P.G., C.R., R.E.; writing—review and editing, E.P., P.G., C.R., R.E.; supervision, E.P., R.E. All authors have read and agreed to the published version of the manuscript.

**Funding:** This research received no external funding.

**Data Availability Statement:** The datasets presented in this article are not readily available because of technical limitations. Requests to access the datasets should be directed to Eugenia Pechkova, eugenia.pechkova@gmail.com.

**Acknowledgments:** The authors appreciate the help of group of Petra Fromme at Biodesign Center for Applied Structural Discovery, Arizona State University for the XFEL experiments at SLAC National Accelerator Laboratory, USA. We are grateful to John Spence, Department of Physics, Arizona State University for LB instrumentation. We also would like to thank Raimund Fromme, ASU for his courtesy of supplying of phycocyanin protein.

**Conflicts of Interest:** Authors declare no conflict of interest.



## References

1. Fromme, P.; Fromme, R.; Blankenship, R.E. Structure and function of photosynthetic complexes in cyanobacteria: A structural and functional perspective. *Photosynth. Res.* **2003**, *77*, 161–178.
2. MacColl, R. Cyanobacterial phycobilisomes. *J. Struct. Biol.* **1998**, *124*, 311–334. [[CrossRef](#)] [[PubMed](#)]
3. Bryant, D.A.; Cohen-Bazire, G. The structure of cyanobacterial phycobilisomes: A model. *Arch. Microbiol.* **1981**, *129*, 273–279. [[CrossRef](#)]
4. Adir, N. Elucidation of the molecular structures of components of the phycobilisome: Reconstructing a giant. *Photosynth. Res.* **2005**, *85*, 15–32. [[CrossRef](#)]
5. Jiang, L.; Wang, Y.; Yin, Q.; Liu, G.; Liu, H.; Huang, Y.; Li, B. Phycocyanin: A Potential Drug for Cancer Treatment. *J. Cancer* **2017**, *8*, 3416–3429. [[CrossRef](#)]
6. Pechkova, E.; Nicolini, C.; Fiordoro, S.; Riekkel, C. Mesoscale ordering of Phycocyanin molecules in Langmuir-Blodgett multilayers. *Langmuir* **2022**, *38*, 86–91. [[CrossRef](#)]
7. Pechkova, E. Light-harvesting proteins intermolecular order in the Langmuir-Blodgett (LB) nanofilms—Methods and applications. *J. Phys. Conf. Ser.* **2023**, *2579*, 012010. [[CrossRef](#)]
8. Pechkova, E.; Nicolini, C. Langmuir-Blodgett Protein Multilayer Nanofilms by XFEL. *NanoWorld J.* **2018**, *4*, 48–53. [[CrossRef](#)]
9. Pechkova, E.; Tripathi, S.; Nicolini, C. MicroGISAXS of LB protein films: Effect of temperature on long-range order. *J. Synchrotron Radiat.* **2009**, *16*, 330–335. [[CrossRef](#)]
10. Nicolini, C.; John, W.; Pechkova, E. Synchrotron Diffraction of Multilayered LS PGA Films after Heating and Cooling. *Nanoworld J.* **2015**, *1*, 4–8. [[CrossRef](#)]
11. Pechkova, E.; Nicolini, C.; Burghammer, M.; Riekkel, C. Emergence of amyloidic fibrillation in 2D-ordered Langmuir-Blodgett protein multilayers upon heating. *Appl. Phys. Lett.* **2020**, *117*, 053701. [[CrossRef](#)]
12. Pagels, F.; Guedes, A.M.; Moreira, F.C. Thermal stability and aggregation of C-phycocyanin: A light scattering and fluorescence study. *J. Mol. Struct.* **2019**, *1181*, 16–22.
13. Fromme, P.; Spence, J.C.H. Femtosecond nanocrystallography using X-ray lasers for membrane protein structure determination. *Curr. Opin. Struct. Biol.* **2011**, *21*, 509–516. [[CrossRef](#)] [[PubMed](#)]
14. Chapman, H.N.; Fromme, P.; Barty, A.; White, T.A.; Kirian, R.A.; Aquila, A.; Hunter, M.S.; Schulz, J.; DePonte, D.P.; Weierstall, U.; et al. Femtosecond X-ray protein nanocrystallography. *Nature* **2011**, *470*, 73–77. [[CrossRef](#)]
15. Kupitz, C.; Basu, S.; Grotjohann, I.; Fromme, R.; Zatsepin, N.A.; Rendek, K.N.; Hunter, M.S.; Shoeman, R.L.; White, T.A.; Wang, D.; et al. Serial time-resolved crystallography of photosystem II using a femtosecond X-ray laser. *Nature* **2014**, *513*, 261–265. [[CrossRef](#)]
16. Martiel, I.; Muller-Werkmeister, H.M.; Cohen, A.E. Strategies for sample delivery for femtosecond crystallography. *Acta Crystallogr. D Struct. Biol.* **2019**, *75*, 160–177. [[CrossRef](#)]
17. Weierstall, U.; Doak, R.B.; Spence, J.C.H.; Starodub, D.; Shapiro, D.; Kennedy, P.; Warner, J.; Hembree, G.G.; Fromme, P.; Chapman, H.N. Droplet streams for serial crystallography of proteins. *Exp. Fluids* **2008**, *44*, 675–689. [[CrossRef](#)]
18. Liu, W.; Wacker, D.; Gati, C.; Han, G.W.; James, D.; Wang, D.; Nelson, G.; Weierstall, U.; Katritch, V.; Barty, A.; et al. Serial femtosecond crystallography of G protein-coupled receptors. *Science* **2013**, *342*, 1521–1524. [[CrossRef](#)]
19. Weierstall, U.; James, D.; Wang, C.; White, T.A.; Wang, D.; Liu, W.; Spence, J.C.H.; Doak, R.B.; Nelson, G.; Fromme, P.; et al. Lipidic cubic phase injector facilitates membrane protein serial femtosecond crystallography. *Nat. Commun.* **2014**, *5*, 3309. [[CrossRef](#)]
20. Frank, M.; Carlson, D.B.; Hunter, M.S.; Williams, G.J.; Messerschmidt, M.; Zatsepin, N.A.; Barty, A.; Benner, W.H.; Chu, K.; Graf, A.T.; et al. Femtosecond X-ray diffraction from two-dimensional protein crystals. *IUCr* **2014**, *1*, 95–100. [[CrossRef](#)]
21. Casadei, C.M.; Tsai, C.-J.; Barty, A.; Hunter, M.S.; Zatsepin, N.A.; Padeste, C.; Capitani, G.; Benner, W.H.; Boutet, S.; Hau-Riege, S.P.; et al. Resolution extension by image summing in SFX of two-dimensional membrane-protein crystals. *IUCr* **2018**, *5*, 103–117. [[CrossRef](#)] [[PubMed](#)]
22. Hunter, M.S.; Segelke, B.; Messerschmidt, M.; Williams, G.J.; Zatsepin, N.A.; Barty, A.; Benner, W.H.; Carlson, D.B.; Coleman, M.; Graf, A.; et al. Fixed-target protein serial micro crystallography with an X-ray free electron laser. *Sci. Rep.* **2014**, *4*, 6026. [[CrossRef](#)] [[PubMed](#)]
23. Opara, N.; Martiel, I.; Arnold, S.A.; Braun, T.; Stahlberg, H.; Makita, M.; David, C.; Padeste, C. Direct protein crystallization on ultrathin membranes for diffraction measurements at X-ray free-electron lasers. *J. Appl. Crystallogr.* **2017**, *50*, 909–918. [[CrossRef](#)]
24. Yoon, C.H.; White, T.A. Climbing the Data Mountain: Processing of SFX Data. In *X-ray Free Electron Lasers*; Boutet, S., Fromme, P., Hunter, M., Eds.; Springer International Publishing: Cham, Switzerland, 2018; ISBN 978-3-030-00550-4. [[CrossRef](#)]
25. Barty, A.; Kirian, R.A.; Maia, F.R.; Hantke, M.; Yoon, C.H.; White, T.A.; Chapman, H. Cheetah: Software for high-throughput reduction and analysis of serial femtosecond X-ray diffraction data. *J. Appl. Crystallogr.* **2014**, *47*, 1118–1131. [[CrossRef](#)]
26. Mariani, V.; Morgan, A.; Yoon, C.H.; Lane, T.J.; White, T.A.; O’Grady, C.; Kuhn, M.; Aplin, S.; Koglin, J.; Barty, A.; et al. OnDA: Online data analysis and feedback for serial X-ray imaging. *J. Appl. Crystallogr.* **2016**, *49*, 1073–1080. [[CrossRef](#)]
27. Sauter, N.K.; Hattne, J.; Grosse-Kunstleve, R.W.; Echols, N. New Python-based methods for data processing. *Acta Crystallogr. D Struct. Biol.* **2013**, *69*, 1274–1282. [[CrossRef](#)]
28. Lyubimov, A.Y.; Uervirojnangkoorn, M.; Zeldin, O.B.; Brewster, A.S.; Murray, T.D.; Sauter, N.K.; Berger, J.M.; Weis, W.I.; Brunger, A.T. IOTA: Integration optimization, triage and analysis tool for the processing of XFEL diffraction images. *J. Appl. Crystallogr.* **2016**, *49*, 1057–1064. [[CrossRef](#)]

29. Foucar, L. CFEL-ASG Software Suite (CASS): Usage for free-electron laser experiments with biological focus. *J. Appl. Crystallogr.* **2016**, *49*, 1336–1346. [[CrossRef](#)]
30. Shin, H.; Kim, S. Data Analysis using Psocake at PAL-XFEL. *J. Korean Phys. Soc.* **2018**, *73*, 16–20. [[CrossRef](#)]
31. Fromme, R.; Ishchenko, A.; Metz, M.; Chowdhury, S.R.; Basu, S.; Boutet, S.; Fromme, P.; White, T.A.; Barty, A.; Spence, J.C.H.; et al. Serial femtosecond crystallography of soluble proteins in lipidic cubic phase. *IUCr* **2015**, *2*, 545–551. [[CrossRef](#)]
32. Roy, D.; Pabbi, S. A simple improved protocol for purification of C-phycoerythrin from overproducing cyanobacteria and its characterization. *J. Appl. Phycol.* **2022**, *34*, 799–810. [[CrossRef](#)]
33. Liang, Y.; Kaczmarek, M.B.; Kasprzak, A.K.; Tang, J.; Shah, M.R.; Jin, P.; Klepacz-Smółka, A.; Cheng, J.J.; Ledakowicz, S.; Daroch, M. Thermosynechococcaceae as a source of thermostable C-phycoerythrins: Properties and molecular insights. *Algal Res.* **2018**, *35*, 223–235. [[CrossRef](#)]
34. Pumas, C.; Vacharapiyasophon, P.; Peerapornpisal, Y.; Leelapornpisid, P.; Boonchum, W.; Ishii, M.; Khanongnuch, C. Thermostability of phycobiliproteins and antioxidant activity from four thermotolerant cyanobacteria. *Phycol. Res.* **2011**, *59*, 166–174. [[CrossRef](#)]
35. Pechkova, E.; Ghisellini, P.; Fiordoro, S.; Rando, C.; Eggenhöfner, R. Insights into Early Phases of Phycocyanin Crystal Formation via SONICC Spectroscopy. *Crystals* **2024**, *14*, 395. [[CrossRef](#)]
36. Bettotti, P. Hybrid Materials for Integrated Photonics. *Adv. Opt.* **2014**, *2024*, 891395. [[CrossRef](#)]
37. Koons, G.L.; Diba, M.; Mikos, A.G. Materials design for bone-tissue engineering. *Nat. Rev. Mater.* **2020**, *5*, 584–603. [[CrossRef](#)]

**Disclaimer/Publisher’s Note:** The statements, opinions and data contained in all publications are solely those of the individual author(s) and contributor(s) and not of MDPI and/or the editor(s). MDPI and/or the editor(s) disclaim responsibility for any injury to people or property resulting from any ideas, methods, instructions or products referred to in the content.